Investigation of ^{10}Be and its cluster dynamics with the nonlocalized clustering approach

Mengjiao Lyu,[1,2,*] Zhongzhou Ren,[1,3,†] Bo Zhou,[4,‡] Yasuro Funaki,[5] Hisashi Horiuchi,[2,6] Gerd Röpke,[7] Peter Schuck,[8,9] Akihiro Tohsaki,[2] Chang Xu,[1] and Taiichi Yamada[10]

[1]*School of Physics and Key Laboratory of Modern Acoustics, Institute of Acoustics, Nanjing University, Nanjing 210093, China*
[2]*Research Center for Nuclear Physics (RCNP), Osaka University, Osaka 567-0047, Japan*
[3]*Center of Theoretical Nuclear Physics, National Laboratory of Heavy-Ion Accelerator, Lanzhou 730000, China*
[4]*Faculty of Science, Hokkaido University, Sapporo 060-0810, Japan*
[5]*Nishina Center for Accelerator-Based Science, Institute of Physical and Chemical Research (RIKEN), Wako 351-0198, Japan*
[6]*International Institute for Advanced Studies, Kizugawa 619-0225, Japan*
[7]*Institut für Physik, Universität Rostock, D-18051 Rostock, Germany*
[8]*Institut de Physique Nucléaire, Université Paris-Sud, IN2P3-CNRS, UMR 8608, F-91406, Orsay, France*
[9]*Laboratoire de Physique et Modélisation des Milieux Condensés, CNRS-UMR 5493, F-38042 Grenoble Cedex 9, France*
[10]*Laboratory of Physics, Kanto Gakuin University, Yokohama 236-8501, Japan*

(Received 24 December 2015; revised manuscript received 4 April 2016; published 5 May 2016)

We extend the concept of nonlocalized clustering to the nucleus ^{10}Be with proton number $Z = 4$ and neutron number $N = 6$ ($N = Z + 2$). The Tohsaki-Horiuchi-Schuck-Röpke (THSR) wave function is formulated for the description of different structures of ^{10}Be. Physical properties such as energy spectrum and root-mean-square radii are calculated for the first two 0^+ states and corresponding rotational bands. With only one single THSR wave function, the calculated results show good agreement with other models and experimental values. We apply, for the first time, the THSR wave function on the chain orbit (σ-orbit) structure in the 0_2^+ state of ^{10}Be. The ring-orbit (π-orbit) and σ-orbit structures are further illustrated by calculating the density distribution of the valence neutrons. We also investigate the nonlocalized dynamics of α clusters and the correlations of two valence neutrons in ^{10}Be.

DOI: 10.1103/PhysRevC.93.054308

I. INTRODUCTION

Cluster formation plays a fundamental role in understanding the structure and properties of nuclei. In recent years, tremendous progress has been made in the investigation of cluster structure in light nuclei [1–13], especially due to the model wave function with nonlocalized clustering concept, namely the Tohsaki-Horiuchi-Schuck-Röpke (THSR) wave function [1–8]. The THSR wave function was first proposed to describe the α-cluster condensation in gaslike states, including the famous Hoyle state (0_2^+ state) in ^{12}C [1]. Then it was successfully applied to various other aggregates of α clusters such as ^{8}Be , ^{16}O , and ^{20}Ne [1–3] and also to one-dimensional chain systems [5]. It was found that one single THSR wave function is almost 100% equivalent to the resonating group method–generator coordinate method (RGM-GCM) wave functions for both gaslike and nongaslike states. In the recent studies of inversion-doublet bands of ^{20}Ne [6,7], the nonlocalized character of clustering rooted in the THSR wave function is proved to be a very important property for clustering structure in light nuclei. Therefore it is very necessary to investigate the nonlocalized cluster dynamics in other different nuclear systems.

In recent years, there are also investigations using the THSR wave function and its intrinsic container structure for nuclei beyond traditional α aggregates. This starts with the calculation of ^{13}C with a neutron probe interacting with the 3α condensation [14]. Also, in this year, the $2\alpha + \Lambda$ system is investigated with the hyper-THSR wave function, which shows the essential role of the container picture for the cluster structure in $^{9}_{\Lambda}$Be [15]. In our previous work, the THSR wave function is constructed with intrinsic negative parity and applied in the calculation of nucleus ^{9}Be with proton number $Z = 4$ and neutron number $N = 5$ ($N = Z + 1$) [8]. In this study, the nonlocalized clustering concept is shown to prevail in the π orbit for ^{9}Be.

In order to apply the nonlocalized clustering concept to more general nuclei, it is very interesting to extend the THSR wave function to the investigation of the $N = Z + 2$ cluster nucleus ^{10}Be in which one more valence neutron is added to the ^{9}Be system. The nucleus ^{10}Be is well known for its typical nuclear molecular orbit structure and has been studied with many different models [16–23]. The 0_2^+ state of ^{10}Be is considered to be an intruder state, which is difficult to describe by simple shell-model methods [19]. Besides, a chain structure with σ binding and enormous spatial extension is found in this 0_2^+ state [17,18]. Another interesting topic for the $N = Z + 2$ nucleus ^{10}Be is the correlation between valence neutrons [20]. Recently, predictions of the 0_3^+ and 0_4^+ states [21] and the existence of $\alpha + t + t$ structure in ^{10}Be [22] have been reported. In the present work, we construct THSR wave functions for ^{10}Be based on the new nonlocalized picture. With these THSR wave functions, we can well describe not only the physical properties of different states of ^{10}Be but also the cluster dynamics in these states with only one single THSR wave function.

*mengjiao_lyu@hotmail.com
†zren@nju.edu.cn
‡bo@nucl.sci.hokudai.ac.jp

We organize this paper as follows. In Sec. II we formulate the THSR wave function for both π and σ binding of ^{10}Be. In Sec. III, we present our results for the $0_1{}^+$ ground state of ^{10}Be and its rotational bands. In Sec. IV, we investigate the $0_2{}^+$ state of ^{10}Be and its σ-orbit structure. In Sec. V, we discuss the nonlocalized α-cluster dynamics and correlations between valence neutrons in these states. Section VI contains the conclusions.

II. FORMULATION OF THE THSR WAVE FUNCTION FOR ^{10}Be

We first introduce the THSR wave function of ^{10}Be for the π-orbit binding structure. There are two valence neutrons in ^{10}Be nucleus and the dineutron correlation should be taken into consideration for nuclei with two valence nucleons such as ^{6}He and ^{10}Be, as discussed previously in Ref. [20]. The introduction of correlations in the THSR wave function is very natural, because the original THSR wave function of α aggregates describes very well the α-α correlations, especially in Refs. [6,7]. Thus, we can describe the correlation of two valence neutrons with a new THSR integration in analogy to what we used for two α clusters.

As shown in Fig. 1(a), the motion and correlation of two valence neutrons are described by generator coordinates $\mathbf{R}_{\rm pair}$ and $\mathbf{R}_n$, where the first one is shared by two valence neutrons because of the dineutron correlation and latter one is different for each neutron. With these generator coordinates, we can write the THSR wave function with dineutron correlation in ^{10}Be as

$$|\Phi(^{10}\mathrm{Be})\rangle = (C_\alpha^\dagger)^2 c_{\rm pair}^\dagger |\mathrm{vac}\rangle, \tag{1}$$

where $C_\alpha^\dagger$ and $c_{\rm pair}^\dagger$ are creation operators of α clusters and dineutron pair, respectively. The α creator $C_\alpha^\dagger$ determines the dynamics of the α clusters and can be written as

$$C_\alpha^\dagger = \int d^3\mathbf{R} \exp\left(-\frac{R_x^2}{\beta_{\alpha,xy}^2} - \frac{R_y^2}{\beta_{\alpha,xy}^2} - \frac{R_z^2}{\beta_{\alpha,z}^2}\right) \int d^3\mathbf{r}_1 \ldots d^3\mathbf{r}_4 \psi(\mathbf{r}_1 - \mathbf{R}) a_{\sigma_1,\tau_1}^\dagger(\mathbf{r}_1) \ldots \psi(\mathbf{r}_4 - \mathbf{R}) a_{\sigma_4,\tau_4}^\dagger(\mathbf{r}_4), \tag{2}$$

where $\mathbf{R}$ is the generator coordinate of the α cluster and $\mathbf{r}_i$ is the position of the ith nucleon. $a_{\sigma,\tau}^\dagger(\mathbf{r}_i)$ is the creation operator of the ith nucleon with spin σ and isospin τ at position $\mathbf{r}_i$. $\psi(\mathbf{r}) = (\pi b^2)^{-3/4} \exp(-r^2/2b^2)$ is the wave function of a single nucleon in the α clusters with a Gaussian form where the parameter b in this Gaussian describes the size of α clusters. $\beta_{\alpha,xy}$ and $\beta_{\alpha,z}$ are parameters for the nonlocalized motion of two α clusters in horizontal or vertical directions respectively, which are shown as a dashed ellipses in Fig. 1.

The dineutron creation operator $c_{\rm pair}^\dagger$ can be denoted as

$$c_{\rm pair}^\dagger = \int d^3\mathbf{R}_{\rm pair} \exp\left(-\frac{R_{{\rm pair},x}^2}{\beta_{{\rm pair},xy}^2} - \frac{R_{{\rm pair},y}^2}{\beta_{{\rm pair},xy}^2} - \frac{R_{{\rm pair},z}^2}{\beta_{{\rm pair},z}^2}\right) \times c_{n,\uparrow}^\dagger(\mathbf{R}_{\rm pair}) c_{n,\downarrow}^\dagger(\mathbf{R}_{\rm pair}). \tag{3}$$

This integration of $\mathbf{R}_{\rm pair}$ describes the correlated motion of two valence neutrons, which is shown as the big solid ellipse in Fig. 1(a). $\beta_{{\rm pair},xy}$ and $\beta_{{\rm pair},z}$ are parameters for this correlated motion in each direction.

$c_{n,\sigma}^\dagger(\mathbf{R}_{\rm pair})$ is the creation operator for each neutron, which has a similar form as $c_{n,\sigma}^\dagger$ for ^{9}Be in our previous work [8]:

$$c_{n,\sigma}^\dagger(\mathbf{R}_{\rm pair}) = \int d^3\mathbf{R}_n \exp\left(-\frac{R_{n,x}^2}{\beta_{n,xy}^2} - \frac{R_{n,y}^2}{\beta_{n,xy}^2} - \frac{R_{n,z}^2}{\beta_{n,z}^2}\right) \times e^{im\phi(\mathbf{R}_{\rm pair}+\mathbf{R}_n)} \int d^3\mathbf{r}_n (\pi b^2)^{-3/4} \times e^{-\frac{(\mathbf{r}_n - \mathbf{R}_{\rm pair} - \mathbf{R}_n)^2}{2b^2}} a_{\sigma,n}^\dagger(\mathbf{r}_n). \tag{4}$$

Here $\mathbf{R}_n$ is the generator coordinator of the valence neutrons, $\mathbf{r}_n$ is the position of the extra neutron, $a_{\sigma,n}^\dagger(\mathbf{r}_n)$ is the creation operator of the extra neutron with spin σ at position $\mathbf{r}_n$, and $\phi_{\mathbf{R}_n}$ is the azimuthal angle in spherical coordinates $(R(\mathbf{R}_{\rm pair}+\mathbf{R}_n), \theta(\mathbf{R}_{\rm pair}+\mathbf{R}_n), \phi(\mathbf{R}_{\rm pair}+\mathbf{R}_n))$ of $(\mathbf{R}_{\rm pair}+\mathbf{R}_n)$. In this creation operator, the size parameter b of the Gaussian is taken to be the same as that in Eq. (2). This integration of $\mathbf{R}_n$ describes the independent motion of each valence neutron with parameters $\beta_{n,xy}$ and $\beta_{n,z}$, which is shown as small solid ellipse in Fig. 1(a).

In the $\beta_{\rm pair} = 0$ limit, the integration over $\mathbf{R}_{\rm pair}$ in Eq. (3) vanishes and the THSR wave function of ^{10}Be becomes

$$|\Phi(^{10}\mathrm{Be})\rangle = (C_\alpha^\dagger)^2 c_{n,\uparrow}^\dagger(\mathbf{0}) c_{n,\downarrow}^\dagger(\mathbf{0}) |\mathrm{vac}\rangle. \tag{5}$$

This wave function corresponds to independent motions for the two valence neutrons in ^{10}Be nucleus, as shown in Fig. 1(b).

In this wave function, the α clusters are assumed to move freely in the three-dimensional containers described by the β parameters, which correspond to motions with positive parity. For the valence neutrons, the motion is determined by both β parameters and phase factor $e^{im\phi(\mathbf{R}_{\rm pair}+\mathbf{R}_n)}$ in Eq. (4). When

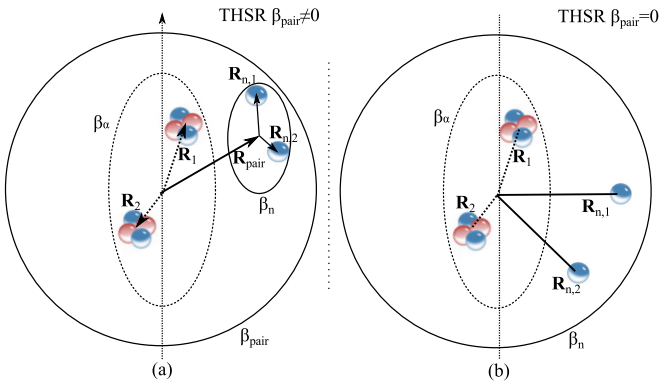

FIG. 1. Generator coordinates and β parameters used in the THSR wave function for the ground state $0_1{}^+$ of ^{10}Be. Left panel (a) shows the case with correlations between valence neutrons. Right panel (b) shows the case of independent valence neutron motion in $\beta_{\rm pair} = 0$ limit. Vectors are corresponding generator coordinates. Dashed ellipses denote nonlocalized motion of α clusters. Solid ellipses denote the nonlocalized motion of the valence neutrons.

$m = \pm 1$, the phase factor $e^{im\phi(\mathbf{R}_{\rm pair}+\mathbf{R}_n)}$ ensures negative parity for the single-nucleon wave function, as illustrated in Ref. [8]. Besides, when $m = 0$, only Gaussian functions are left in the creation operators in Eq. (4), which corresponds to a positive parity for the valence neutrons. Therefore, we have the total parity of ^{10}Be as

$$\pi = \pi_\alpha^{(1)} \times \pi_\alpha^{(2)} \times \pi_n^{(1)} \times \pi_n^{(2)} = \begin{cases} (+)\times(+)\times(+)\times(+) = + & (m_1 = m_2 = 0), \\ (+)\times(+)\times(-)\times(-) = + & (m_1 = 1, m_2 = -1). \end{cases} \quad (6)$$

For the $0_2{}^+$ state of ^{10}Be, it is already known that this state has a very typical chain structure because of the σ-binding mechanism [17,24]. In this structure, valence neutrons stay between or outside of two α clusters along the α-α chain. Also, a recent study shows that α-linear chain structure of ^{12}C and ^{16}O can be well described by the THSR wave function [5]. Thus, we introduce the chain structure assumption and construct the one-dimensional constrained THSR wave function for the $0_2{}^+$ state of ^{10}Be, as

$$|\Phi_{\rm chain}(^{10}{\rm Be})\rangle = (C_\alpha^\dagger)^2 c_{n,\uparrow}^\dagger c_{n,\downarrow}^\dagger |{\rm vac}\rangle. \quad (7)$$

Here the α-creation operator $C_\alpha^\dagger$ is similar to Eq. (2) but operates only on the z axis,

$$C_\alpha^\dagger = \int dR_z \exp\left(-\frac{R_z^2}{\beta_{\alpha,z}^2}\right) \int d^3\mathbf{r}_1 \ldots d^3\mathbf{r}_4 \psi(\mathbf{r}_1 - \mathbf{R}) a_{\sigma_1,\tau_1}^\dagger(\mathbf{r}_1) \ldots \psi(\mathbf{r}_4 - \mathbf{R}) a_{\sigma_4,\tau_4}^\dagger(\mathbf{r}_4), \quad (8)$$

where $\mathbf{R}$ is the generator coordinate of the α cluster on the z axis and $\mathbf{r}_i$ is the position of the ith nucleon. For the valence neutrons, a creation operator with a node structure is constructed for the correct description of the σ orbits, as

$$c_{n,\sigma}^\dagger = \int dR_{n,z}(D - |R_{n,z}|) \exp\left(-\frac{R_{n,z}^2}{\beta_{n,z}^2}\right) \int d^3\mathbf{r}_n \times (\pi b^2)^{-3/4} e^{-\frac{(\mathbf{r}_n - \mathbf{R}_n)^2}{2b^2}} a_{\sigma,n}^\dagger(\mathbf{r}_n). \quad (9)$$

Here, $\mathbf{R}_n$ is the generator coordinate of the valence neutron on the z axis and $\mathbf{r}_n$ is the position of the valence neutron. We introduce a new factor $(D - |R_{n,z}|)$ in this THSR integration to provide a node structure for the wave function of the valence neutrons. Two nodes appear in the wave function when $R_{n,z} = \pm D$, which are locations near the α clusters. As a demonstration, we choose parameter $D = 2$ fm and $\beta_{n,z} = 5$ fm, and show the single-nucleon wave function $\phi_n(z)$ for valence neutron in Fig. 2. It is clearly seen in the figure that the wave function $\phi_n(z)$ has a different sign between the midregion and two flanks. Also, two nodes appear near $z = 2$ fm as expected. In our calculation, the parameter D is treated as a variational parameter to obtain a correct node position for the wave function $\phi_n(z)$.

In this wave function, the α clusters move freely in one-dimensional containers while the motion of valence neutrons is constrained by the node structure above. It is obvious that Eqs. (8) and (9) contain only even functions, so the corresponding parity in this wave function is given by

$$\pi = \pi_\alpha^{(1)} \times \pi_\alpha^{(2)} \times \pi_n^{(1)} \times \pi_n^{(2)} = (+)\times(+)\times(+)\times(+) = +. \quad (10)$$

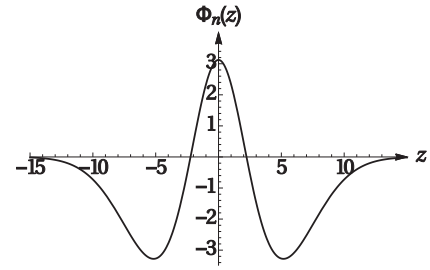

FIG. 2. Single-nucleon wave function $\phi_n(z)$ for the valence neutron in the $0_2{}^+$ state of ^{10}Be. Parameters are chosen as $D = 2$ fm and $\beta_{n,z} = 5$ fm.

In order to eliminate effects from spurious center-of-mass (c.m.) motion, the c.m. part of $|\Phi\rangle$ is projected onto a $(0s)$ state [25]. We use the following transformation of coordinates $\mathbf{r}_i$ in $|\Phi\rangle$ to eliminate the effects of the spurious center-of-mass motion as in Ref. [25]:

$$|\Psi\rangle = |(0s){\rm c.m.}\rangle\rangle\langle\langle(0s){\rm c.m.}|\Phi\rangle. \quad (11)$$

Here $(0s)$ represents the wave function of the c.m. coordinate $\mathbf{X}_G$ in the s state, and the double brackets denote the integration with respect to coordinate $\mathbf{X}_G$. We also apply the angular-momentum projection technique $\hat{P}_{MK}^J|\Psi\rangle$ to restore the rotational symmetry [26],

$$|\Psi^{JM}\rangle = \hat{P}_{MK}^J|\Psi\rangle = \frac{2J+1}{8\pi^2} \int d\Omega D_{MK}^{J*}(\Omega)\hat{R}(\Omega)|\Psi\rangle, \quad (12)$$

where J is the total angular momentum of ^{10}Be.

The Hamiltonian of the ^{10}Be system can be written as

$$H = \sum_{i=1}^{10} T_i - T_{\rm c.m.} + \sum_{i<j}^{10} V_{ij}^N + \sum_{i<j}^{10} V_{ij}^C + \sum_{i<j}^{10} V_{ij}^{ls}, \quad (13)$$

where $T_{\rm c.m.}$ is the kinetic energy of the center-of-mass motion. Volkov No. 2 [27] is used as the central force of the nucleon-nucleon potential,

$$V_{ij}^N = \{V_1 e^{-\alpha_1 r_{ij}^2} - V_2 e^{-\alpha_2 r_{ij}^2}\} \times \{W - M\hat{P}_\sigma \hat{P}_\tau + B\hat{P}_\sigma - H\hat{P}_\tau\}, \quad (14)$$

where $M = 0.6, W = 0.4$, and $B = H = 0.125$. Other parameters are $V_1 = -60.650$ MeV, $V_2 = 61.140$ MeV, $\alpha_1 = 0.309$ fm^{-2}, and $\alpha_2 = 0.980$ fm^{-2}. The G3RS (Gaussian soft-core potential with three ranges) term is taken as the two-body type spin-orbit interaction [28],

$$V_{ij}^{ls} = V_0^{ls}\{e^{-\alpha_1 r_{ij}^2} - e^{-\alpha_2 r_{ij}^2}\}\mathbf{L}\cdot\mathbf{S}\hat{P}_{31}, \quad (15)$$

where $\hat{P}_{31}$ projects the two-body system onto triplet odd state. Parameters in V_{ij}^{ls} are taken from Ref. [21] with $V_0^{ls} = 1600$ MeV, $\alpha_1 = 5.00\,{\rm fm}^{-2}$, and $\alpha_2 = 2.778\,{\rm fm}^{-2}$.

III. THE 0_1^+ GROUND STATE OF ^{10}Be

The Monte Carlo method is used because of its superiority in calculating the numerical integrations in the Hamiltonian kernels, which otherwise is very difficult to solve analytically for the THSR wave functions of ^{10}Be. The Monte Carlo technique is very flexible for extending the THSR concept. The Monte Carlo calculation includes the integrations of Euler angle Ω in the angular momentum projection and integrations of generator coordinates $\{\mathbf{R},\mathbf{R}_n\}$ in the creation operators. When using one single THSR wave function, the numerical calculation would be much more efficient than traditional GCM calculations. To compare our results with other models, the width of the Gaussians in the single-nucleon wave function is chosen to be $b = 1.46$ fm, which is the same as fixed in Refs. [21,29]. The β parameters in the THSR wave functions are treated as variational parameters and are optimized with the variational technique.

We investigate the ground state 0_1^+ of ^{10}Be and its rotational band with both the THSR wave function of ^{10}Be. We choose the parameter $m = 1$ with spin up for one valence neutron and parameter $m = -1$ with spin down for the other. This is to ensure parallel coupling of spin and the orbital angular momentum for both neutrons as we used in previous investigations [8]. The optimum variational parameters for the THSR wave function are $\beta_{\alpha,xy} = 0.1$ fm, $\beta_{\alpha,z} = 2.0$ fm, $\beta_{\mathrm{pair},xy} = 0.8$ fm, $\beta_{\mathrm{pair},z} = 1.8$ fm, $\beta_{n,xy} = 2.0$ fm, and $\beta_{n,z} = 2.7$ fm. We also obtain results with the $\beta_{\mathrm{pair}} = 0$ limit, and the corresponding optimum variational parameters are $\beta_{\alpha,xy} = 0.1$ fm, $\beta_{\alpha,z} = 2.0$ fm, $\beta_{n,xy} = 2.0$ fm, and $\beta_{n,z} = 3.5$ fm.

In Table I, we list the calculated results of the 0^+ ground state of ^{10}Be together with results from other models and experimental values. The binding energies obtained for the ground state 0_1^+ is -58.2 MeV with the THSR wave functions. When we take the $\beta_{\mathrm{pair}} = 0$ limit, the binding energy obtained is -58.0 MeV. Theoretical calculations with other models, in which the same potential is used, provide binding energies of the ground state of ^{10}Be ranging from about -59 MeV to -60 MeV, which is about 1–2 MeV lower than our results [20,29]. This difference is reasonable because we are using only one single THSR wave function, which may not be the optimal choice for the valence neutrons. If we superpose 8 THSR wave functions with different parameters β for α clusters or valence neutrons in the THSR wave function, the ground-state energy would decrease to -59.0 MeV, which is consistent with other methods, as shown in Table I. The experimental value for the ground state of ^{10}Be is -65.0 MeV, which is much lower than any theoretical results from our and other groups' works. These differences originate from the choice of effective potentials.

TABLE I. Results obtained for the 0^+ ground state of ^{10}Be. THSR denotes binding energy calculated with the THSR wave function. THSR ($\beta_{\mathrm{pair}} = 0$) denotes binding energy calculated with the THSR wave function and the $\beta_{\mathrm{pair}} = 0$ limit. $\mathrm{THSR}_{\Sigma 8}$ denotes calculated result by superposing 8 different THSR wave functions. Results from other theoretical methods are also listed.

Model	E (MeV)
THSR	-58.2
THSR ($\beta_{\mathrm{pair}} = 0$)	-58.0
$\mathrm{THSR}_{\Sigma 8}$	-59.0
AMD [20]	-58.7
AMD+DC [20]	-60.4
AMD+GCM [29]	-59.2

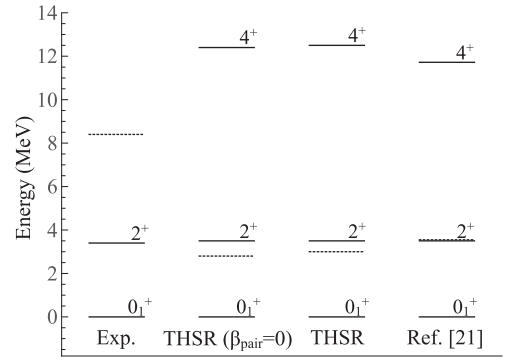

FIG. 3. The 0^+ ground state of ^{10}Be and its rotational band. "THSR" denotes calculated results with the THSR wave function. "THSR ($\beta_{\mathrm{pair}} = 0$)" denotes calculated results with the THSR wave function and the $\beta_{\mathrm{pair}} = 0$ limit. "Ref. [21]" denotes the results of the AMD method [21]. "Exp." denotes the experimental result. The dashed lines indicate the corresponding $\alpha + \alpha + n + n$ threshold -55.2 MeV.

From these results, we can also notice that the binding energy of the ground state is improved by about 0.2 MeV by the introduction of the valence neutron correlation in the THSR wave function. This improvement shows the correlation effect of the valence neutrons in the ground state, as we will discuss later in Sec. V.

In our present calculation, the ansatz of Gaussians (multiplied by factors) is used for the valence neutron in the THSR wave functions. In the future, we will discuss more general form of the THSR wave function for a better optimized description of the valence neutrons.

We show in Fig. 3 the energy spectrum of the 0_1^+ rotational band of ^{10}Be based on the ground state. The calculated excitation energy of the 2_1^+ state is 3.5 MeV and fits very well with the experimental value 3.4 MeV. Good agreement can also be seen between our calculation and the AMD method for the 2_1^+ and 4_1^+ excited states.

The root-mean-square radius of the 0_1^+ ground state of ^{10}Be is also obtained from our approach. The result is 2.57 fm with one single THSR wave function, which is consistent with the value 2.5 fm from Ref. [21], but slightly larger than the value 2.37 fm from Ref. [20] and the experimental value 2.30 fm. This small difference originates from the slightly weaker binding effect described by only one single THSR wave function, as discussed above.

The density distribution $\rho(\mathbf{r}_n')$ of the extra nucleons is calculated to give a clear view of the dynamics of the valence neutrons. The intrinsic wave function $|\Psi\rangle$ of ^{10}Be can be

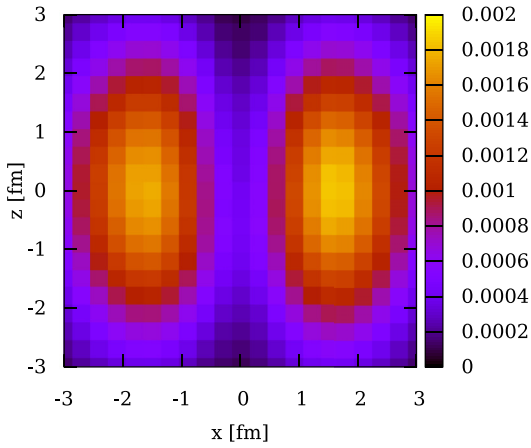

FIG. 4. Density distribution of the valence neutrons in the intrinsic ground state of ^{10}Be. The color scale of each point in the figure is proportional to the nucleon density on the x-z plane of the $y = 0$ cross section. The unit of the density is fm^{-3}.

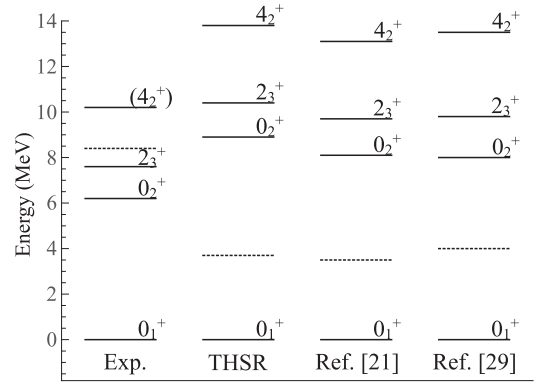

FIG. 5. Energy spectrum of the 0_2^+ rotational band relative to the ground-state energy. The one labeled with Ref. [21] is the value calculated with the AMD+DC method [21]. The one labeled with Ref. [29] is the value calculated with the $\beta - \gamma$ constrained AMD+GCM method [29]. The dashed lines are the corresponding $\alpha + \alpha + n + n$ thresholds of -55.2 MeV.

written in the following form:

$$|\Psi\rangle = \mathrm{C}\mathcal{A}[\Phi^{\mathrm{THSR}}(2\alpha)\phi_{\mathrm{pair}}(\mathbf{r}_{n,1},\mathbf{r}_{n,2})], \tag{16}$$

where $\mathcal{A}$ is the antisymmetrizer and C is a normalization constant. Then the density distribution $\rho(\mathbf{n},\mathbf{r}')$ of the valence neutrons is defined as

$$\rho(\mathbf{r}'_n) = N_c\langle\Phi^{\mathrm{THSR}}(2\alpha)\phi_{\mathrm{pair}}(\mathbf{r}_{n,1},\mathbf{r}_{n,2})|\delta(\mathbf{r}_{n,1} - \mathbf{X}_G - \mathbf{r}'_n) + \delta(\mathbf{r}_{n,2} - \mathbf{X}_G - \mathbf{r}'_n)|\Psi\rangle, \tag{17}$$

where N_c is the normalization constant [30]. As shown in Fig. 4, the density distribution of two valence neutrons has the same shape as the one which we obtained for the ground state ^{9}Be [8] with only a single valence neutron. The extension of the density distribution in the z direction and the absence of neutrons along the z axis shows a good description of the π orbit in the ground state of ^{10}Be as suggested by nuclear molecular orbit (MO) model [16,17]. This reproduction of π-orbit structure is obtained naturally from the antisymmetrization in the THSR wave function, which cancels nonphysical distribution of valence neutrons, e.g., positions close to the center of α clusters.

IV. THE 0_2^+ CHAIN STATE OF ^{10}Be

In this section we study the 0_2^+ state of ^{10}Be with one single THSR wave function as shown in Eq. (7). The optimum parameter D in Eq. (9) is $D = 2.0$ fm. Other optimum variational parameters in the THSR wave function are $\beta_\alpha = 3.5$ and $\beta_n = 4.0$ fm. The calculated spectrum for the 0_2^+ rotational band based on the ground state is shown in Fig. 5. The ground-state energy from THSR calculation in this figure is chosen to be the one with -59.0 MeV obtained from the superposed THSR wave functions as listed in Table I. Figure 5 shows systematical discrepancies between theoretical results calculated by different models and the experimental values. This is because of the choice of effective interactions. The calculated energy spectrum of the 0_2^+ rotational band with the THSR wave function, as shown in Fig. 5, agrees well with results of other theoretical models from Refs. [21,29]. The THSR wave function also gives energy gaps between the states in the 0_2^+ band which fit very well with experimental data and other models. It is very interesting to see that one single THSR wave function can describe well the 0_2^+ state of ^{10}Be, while in other theoretical models superposition of large number of basis sets is needed.

We checked the orthogonality between the THSR wave function for the 0_2^+ state and the 0_1^+ ground state. The calculated overlap between these two states is 1.4%, which satisfies the requirement for eigenstates.

We also calculate the root-mean-square radius for the 0_2^+ state of ^{10}Be. The calculated result is 3.11 fm, which is consistent with 2.96 fm from Ref. [20] and 3.4 fm from Ref. [21].

To illustrate the structure of the 0_2^+ state of ^{10}Be with the THSR wave function, we show the density distribution $\rho(\mathbf{r}'_n)$ of valence nucleons in Fig. 6. This distribution demonstrates

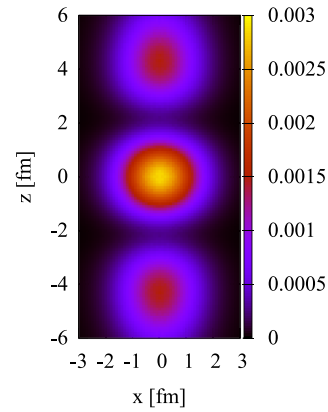

FIG. 6. Density distribution of valence neutrons in the intrinsic 0_2^+ state of ^{10}Be. The color scale of each point in the figure is proportional to the nucleon density in the x-z plane of the $y = 0$ cross section. The unit of the density is fm^{-3}.

similar characteristics after antisymmetrization as the wave function of a single valence neutron in Fig. 2. It is clearly seen that the distribution of valence neutrons is divided into three regions separated by two nodes perpendicular to the z axis, which is a typical characteristic of the σ orbit. The node structure originates from the newly introduced factor $(D - |R_{n,z}|)$ in Eq. (9). Also a large spread of more than 10 fm along the z axis is observed for the valence neutrons, which is one of the reasons for the enormously large spatial extension of the $0_2{}^+$ state in ^{10}Be. Another reason is the large α-cluster distribution as discussed in the next section.

V. ANALYSIS OF CLUSTER DYNAMICS AND DINEUTRON CORRELATIONS

In this section, we discuss the dynamics of the α clusters and the valence neutrons. The THSR wave function describes the α-cluster motion by a Gaussian style THSR integration of generator coordinates as in Eqs. (2) or (8). The optimum β parameters in the α-creation operators are $\beta_{\alpha,xy} \approx 0$ fm, $\beta_{\alpha,z} = 2.0$ fm for the ground $0_1{}^+$ state while the optimum value $\beta_\alpha = 4.0$ fm is obtained for the $0_2{}^+$ state. Considering that large β parameters correspond to large extension of the nonlocalized cluster motion, it is clear that the α particles are much more tightly bound by the π orbit than by the σ orbit. The π-binding effect in the ground state of ^{10}Be is also stronger than that in the ground state of ^{9}Be, where the optimum parameter for α cluster is $\beta_{\alpha,z} = 4.2$ fm [8].

In our calculation, the THSR wave function for ^{10}Be is based on the nonlocalized picture of cluster dynamics. It is thus interesting and important to study whether this nonlocalized concept prevails for the 0^+ states of ^{10}Be. Here we follow the scheme of hybrid wave function that was first introduced by Zhou *et al.* in the discovery of nonlocalized clustering dynamics [6]. We formulate the hybrid wave function of ^{10}Be as

$$C_\alpha^\dagger = \int d^3\mathbf{R} \exp\left(-\frac{R_x^2}{\beta_{\alpha,xy}^2} - \frac{R_y^2}{\beta_{\alpha,xy}^2} - \frac{R_z^2}{\beta_{\alpha,z}^2}\right) \int d^3\mathbf{r}_1 \ldots d^3\mathbf{r}_4 \times \psi(\mathbf{r}_1 - \mathbf{R} \pm \mathbf{S}) a_{\sigma_1,\tau_1}^\dagger(\mathbf{r}_1) \ldots \psi(\mathbf{r}_4 - \mathbf{R} \pm \mathbf{S}) a_{\sigma_4,\tau_4}^\dagger(\mathbf{r}_4). \quad (18)$$

Here $\mathbf{S}$ is an introduced generator coordinate. Operator $\pm$ is chosen to be $+$ for the first α cluster and $-$ for the other α cluster. When $\beta = 0$, the wave function for α clusters becomes a simple Brink wave function, and $\mathbf{S}$ represents half of the intercluster distance of two α clusters. When $\mathbf{S} = 0$, the wave function reduced into the standard THSR wave function as we used previously. In other cases, the wave function becomes a hybrid of the localized Brink wave function and the nonlocalized THSR wave function. By variational optimization of parameter β and generator coordinate $\mathbf{S}$, the nonlocalized dynamics in the two 0^+ states of ^{10}Be can be illustrated. Because the variational result in Sec. III shows extreme deformation for the intrinsic wave function before angular momentum projection, we only need to discuss the α-cluster dynamics along the z axis.

In Fig. 7 we show the energy curves with different parameter β_z for the α-cluster motion in the hybrid wave function. For the

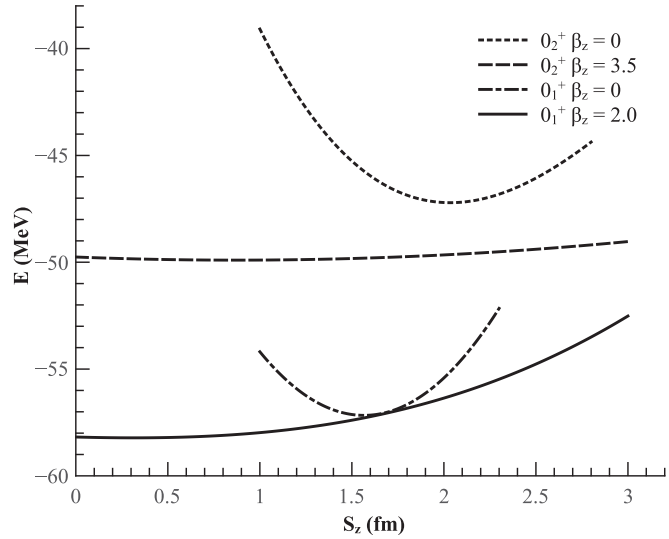

FIG. 7. Energy curves with different parameter β_z for the α-cluster motion in the hybrid wave function.

curves with $\beta_{\alpha,z} = 0$, which corresponds to the Brink model, the minimum energy locates at nonzero value for S_z. This seems to suggest a localized clustering dynamics, with the distance of two α clusters around 3.2 fm for the $0_1{}^+$ ground state and 4.0 fm for the $0_2{}^+$ excited state. However, when we take $\beta_{\alpha,z} = 2.0$ fm and 3.5 fm for the $0_1{}^+$ state and $0_2{}^+$ state respectively, the energy curves shows much lower (1–2 MeV) binding energy at $S_z = 0$. This shows that the nonlocalized model characterized by parameter β provides a better description than the localized picture for these two 0^+ states of ^{10}Be. It is also interesting to find that this model also works for the compact $0_1{}^+$ ground state with a small β parameter $\beta_{\alpha,z} = 2.0$ fm, which shows that the THSR wave function prevails for nongaslike cluster states. This is consistent with a previous study of the compact ground state of ^{20}Ne, where small β parameters are also observed [6]. For these states, localization of α clusters at the SU(3) limit comes from the antisymmetrization because of the fermion nature of nucleons. The localization is not due to dynamic but to kinematic reasons, and the concept of nonlocalized dynamics prevails in this situation [7].

We further compare the fully nonlocalized description and the hybrid description for the 0^+ states. We show in Fig. 8 the contour map of the binding energy of the $0_1{}^+$ ground state of ^{10}Be with different parameters $\beta_{\alpha,z}$ and S_z. We can see two optimum points with value -58.2 MeV on the contour map. The optimum value, which locates along the axis where $S_z = 0$, corresponds to a standard THSR wave function. Squared overlap of 99.87% between these two optimum points is obtained by numerical calculation, which shows that these two points correspond to almost equivalent wave functions. So, we simply choose the simpler one along the $S_z = 0$ axis. We also list in Table II the binding energies of two 0^+ obtained with the Brink wave function, THSR wave function, and also hybrid wave function. The binding energy of the $0_2{}^+$ excited state calculated with THSR wave function is also found to be the lowest one. We can thus conclude from the variational principle

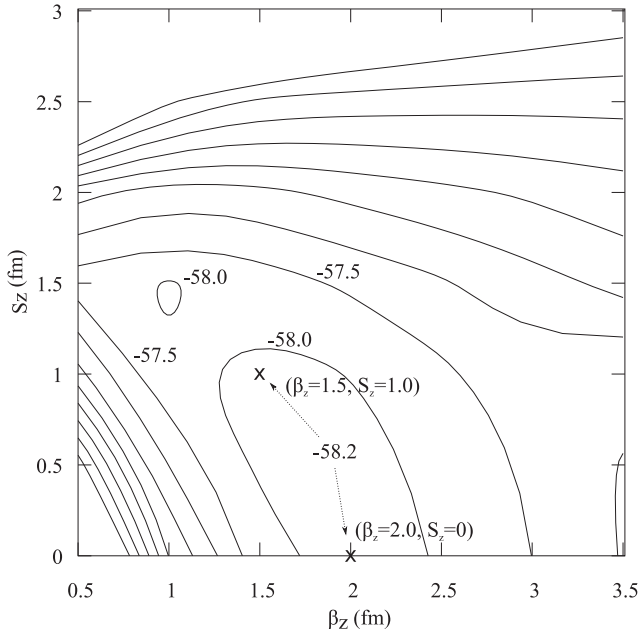

FIG. 8. Contour map of the binding energy of the 0_1^+ ground state of ^{10}Be with different parameters $\beta_{\alpha,z}$ and S_z. Other parameters for α clusters are $\beta_{\alpha,xy} = 0.1$ fm and $S_z = 0$ fm. Parameters for valence neutrons are taken from the variational result in Sec. III. The optimum value is marked on the map labeled with corresponding coordinates.

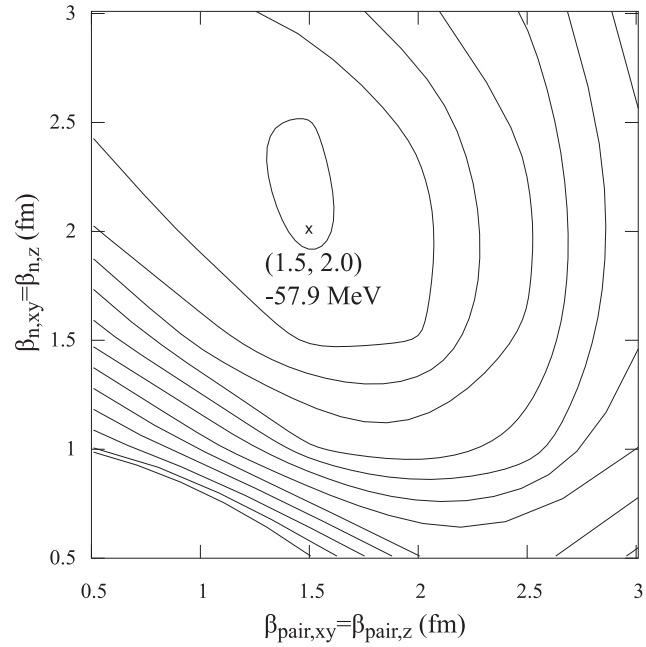

FIG. 9. Contour map of the binding energy surface of the ground state with different β parameters in the THSR wave function. The horizontal coordinates are the β_{pair} parameters as $\beta_{\text{pair},xy} = \beta_{\text{pair},z}$. The vertical coordinates are the β_n parameters as $\beta_{n,xy} = \beta_{n,z}$. Other parameters are $\beta_{\alpha,xy} = 0.1$ fm, $\beta_{\alpha,z} = 2.0$ fm. The optimum value is marked on the map labeled with corresponding coordinates.

that the THSR wave function provides better description for these 0^+ states as a special case of the hybrid description.

Another interesting problem is the dineutron correlation effect in the ^{10}Be nucleus. With the THSR wave function, we calculate the contour map of the binding energy surface for the ground state of ^{10}Be as shown in Fig. 9. For simplicity, we fix the deformation between x, y, and z directions to be 0. The optimum binding energy locates near the coordinates (1.5,2.0), where $\beta_{\text{pair},xy} = \beta_{\text{pair},z} = 1.5$ fm and $\beta_{n,xy} = \beta_{n,z} = 2.0$ fm. This optimum value is slightly higher than the final result of -58.2 MeV because deformation is neglected here. When $\beta_{\text{pair}} = 0$, the THSR wave function turns to describe independent motion for two valence neutrons. Thus, the optimum value of parameter $\beta_{\text{pair}} > 0$ shows the existence of correlation effects in the ground state, as discussed above. A large distance between the two neutrons in the dineutron pair can be concluded because of the big value of the parameter β_n. The small value of the parameter β_{pair} describes relatively weak correlations between two valence neutrons in our calculation. We also study the correlation of the two valence neutrons in the 0_2^+ state of ^{10}Be. A very large value of the parameter β_n and a very small parameter β_{pair} are obtained, which show nearly independent motion of the two valence neutrons in this state.

TABLE II. Binding energies obtained for the 0_1^+ state and 0_2^+ state of ^{10}Be with the hybrid wave function. Binding energies in the first row are calculated with parameter $\beta_z = 0$ and parameter S_z chosen freely, which corresponds to a Brink wave function. Binding energies in the second row are calculated with parameter β_z chosen freely and parameter $S_z = 0$, which corresponds to a THSR wave function. Binding energies in the third row are calculated with parameter β_z and parameter S_z chosen freely.

β_z	S_z	0_1^+	0_2^+
$\beta_z = 0$	S_z free	-57.1	-47.3
β_z free	$S_z = 0$	-58.2	-49.9
β_z free	S_z free	-58.2	-49.9

VI. CONCLUSION

We investigated the $N = Z + 2$ nucleus ^{10}Be from the nonlocalized clustering concept. THSR wave functions with π-orbit structure and chain (σ-orbit) structure are formulated for ^{10}Be. Correct parity and node structures are ensured in THSR wave functions for the corresponding states. The 0_1^+ ground state of ^{10}Be and its rotational band are calculated and the results agree well with other models and experimental values. Small improvement is observed for the binding energy of the ground state with introduction of correlations between two valence neutrons in a single THSR wave function. The 0_2^+ state is also studied with the newly formulated THSR wave function containing a node factor. The calculated energy spectrum of the 0_2^+ rotational band is consistent with values from other models as well as with experiments. This result is very interesting because only one single THSR wave function is used. Root-mean-square radii are also calculated for the first two 0^+ states of ^{10}Be, which have good agreement with other models. The density distribution

of valence neutrons shows good description of the σ orbit by the THSR wave function. It is the first application of the nonlocalized picture to σ-orbit binding systems. Analysis of optimum β parameters shows a much tighter binding effect for α clusters within the π-orbit structure than with the σ-orbit structure. By analyzing energy curves and contour maps for binding energies calculated with the hybrid wave function, we find that the nonlocalized clustering picture prevails for the 0_1^+ state and 0_2^+ state of ^{10}Be. We also discussed the correlation effect between valence neutrons of two valence neutrons in the ground state. The investigation of ^{10}Be is another extension of the nonlocalized concept and of the THSR wave function towards more general nuclear structures. Our calculations with the THSR wave function and the Monte Carlo technique requires less numerical work than the traditional GCM treatment. Also, the THSR wave function used in this work illustrates more physical insights into the ^{10}Be nucleus. In the future, this scheme based on the nonlocalized concept is also promising for the study of neutron-rich nuclei with cluster structures and the investigations of their corresponding cluster and nucleon dynamics.

ACKNOWLEDGMENTS

The authors would like to thank Prof. Kanada-En'yo for valuable discussions. This work is supported by the National Natural Science Foundation of China (Grants No. 11535004, No. 11375086, No. 11120101005, No. 11175085, No. 11235001, No. 11505292, and No. 11575082), by the 973 National Major State Basic Research and Development of China (Grant No. 2013CB834400), and by the Science and Technology Development Fund of Macao (Grant No. 068/2011/A).

[1] A. Tohsaki, H. Horiuchi, P. Schuck, and G. Röpke, Phys. Rev. Lett. **87**, 192501 (2001).
[2] Y. Funaki, H. Horiuchi, A. Tohsaki, P. Schuck, and G. Röpke, Prog. Theor. Phys. **108**, 297 (2002).
[3] Bo Zhou, Zhongzhou Ren, Chang Xu, Yasuro Funaki, Taiichi Yamada, Akihiro Tohsaki, Hisashi Horiuchi, Peter Schuck, and Gerd Röpke, Phys. Rev. C **86**, 014301 (2012).
[4] T. Yamada and P. Schuck, Eur. Phys. J. A **26**, 185 (2005).
[5] T. Suhara, Y. Funaki, B. Zhou, H. Horiuchi, and A. Tohsaki, Phys. Rev. Lett. **112**, 062501 (2014).
[6] Bo Zhou, Yasuro Funaki, Hisashi Horiuchi, Zhongzhou Ren, Gerd Röpke, Peter Schuck, Akihiro Tohsaki, Chang Xu, and Taiichi Yamada, Phys. Rev. Lett. **110**, 262501 (2013).
[7] Bo Zhou, Yasuro Funaki, Hisashi Horiuchi, Zhongzhou Ren, Gerd Röpke, Peter Schuck, Akihiro Tohsaki, Chang Xu, and Taiichi Yamada, Phys. Rev. C **89**, 034319 (2014).
[8] Mengjiao Lyu, Zhongzhou Ren, Bo Zhou, Yasuro Funaki, Hisashi Horiuchi, Gerd Röpke, Peter Schuck, Akihiro Tohsaki, Chang Xu, and Taiichi Yamada, Phys. Rev. C **91**, 014313 (2015).
[9] Y. Kanada-En'yo, H. Horiuchi, and A. Ono, Phys. Rev. C **52**, 628 (1995).
[10] Chang Xu and Zhongzhou Ren, Phys. Rev. C **73**, 041301 (2006).
[11] Yuejiao Ren and Zhongzhou Ren, Phys. Rev. C **85**, 044608 (2012).
[12] Wanbing He, Yugang Ma, X. G. Cao, X. Z. Cai, and G. Q. Zhang, Phys. Rev. Lett. **113**, 032506 (2014).
[13] Zaihong Yang, Yanlin Ye, Z. H. Li, J. L. Lou, J. S. Wang, D. X. Jiang, Y. C. Ge, Q. T. Li, H. Hua, X. Q. Li, F. R. Xu, J. C. Pei, R. Qiao, H. B. You, H. Wang, Z. Y. Tian, K. A. Li, Y. L. Sun, H. N. Liu, J. Chen, J. Wu, J. Li, W. Jiang, C. Wen, B. Yang, Y. Y. Yang, P. Ma, J. B. Ma, S. L. Jin, J. L. Han, and J. Lee, Phys. Rev. Lett. **112**, 162501 (2014).
[14] A. Tohsaki, Int. J. Mod. Phys. E **17**, 2106 (2008).
[15] Y. Funaki, T. Yamada, E. Hiyama, B. Zhou, and K. Ikeda, Prog. Theor. Exp. Phys. **2014**, 113D01 (2014).
[16] W. von Oertzen, Z. Phys. A **354**, 37 (1996).
[17] N. Itagaki and S. Okabe, Phys. Rev. C **61**, 044306 (2000).
[18] M. Ito, K. Kato, and K. Ikeda, Phys. Lett. B **588**, 43 (2004).
[19] E. K. Warburton and B. A. Brown, Phys. Rev. C **46**, 923 (1992).
[20] F. Kobayashi and Y. Kanada-Enyo, Prog. Theor. Phys. **126**, 457 (2011).
[21] F. Kobayashi and Y. Kanada-Enyo, Phys. Rev. C **86**, 064303 (2012).
[22] N. Itagaki, M. Ito, M. Milin, T. Hashimoto, H. Ishiyama, and H. Miyatake, Phys. Rev. C **77**, 067301 (2008).
[23] T. Myo, A. Umeya, H. Toki, and K. Ikeda, Prog. Theor. Exp. Phys. **2015**, 63D03 (2015).
[24] Y. Ogawa, K. Arai, Y. Suzuki, and K. Varga, Nucl. Phys. A **673**, 122 (2000).
[25] S. Okabe, Y. Abe, and H. Tanaka, Prog. Theor. Phys. **57**, 866 (1977).
[26] P. Ring and P. Schuck, *The Nuclear Many-Body Problem* (Springer-Verlag, New York, 1980), p. 474.
[27] A. B. Volkov, Nucl. Phys. **74**, 33 (1965).
[28] N. Yamaguchi, T. Kasahara, S. Nagata, and Y. Akaishi, Prog. Theor. Phys. **62**, 1018 (1979).
[29] T. Suhara and Y. Kanada-Enyo, Prog. Theor. Phys. **123**, 303 (2010).
[30] H. Horiuchi, Prog. Theor. Phys. Supple. **62**, 90 (1977).